Tensorial rheological model for concentrated non-colloidal suspensions: normal-stress differences

Olivier Ozenda, Pierre Saramito, Guillaume Chambon

Tensorial rheological model for concentrated non-colloidal suspensions: normal-stress differences

Olivier Ozenda[1,2] Pierre Saramito[1]† and Guillaume Chambon[2]

[1]Lab. J. Kuntzmann - CNRS and Univ. Grenoble Alpes, CS 40700 - 38058 Grenoble Cedex 9, France

[2]Univ. Grenoble Alpes, IRSTEA, UR ETGR, 2 rue de la Papeterie, 38402 St-Martin-d'Hères, France

(Received xx; revised xx; accepted xx)

Most existing rheological models for non-colloidal suspensions fail to simultaneously capture the two main non-Newtonian trends of these systems, namely finite normal stress differences and transient effects. We address this issue by extending a previously-proposed minimal model accounting for microstructure anisotropy through a conformation tensor, and which was shown to correctly predict transient effects (Ozenda *et al.* 2018). The new model is compared to a large experimental dataset involving varying volume fractions, from dilute to concentrated cases. Both transient evolution of apparent viscosity during shear reversal, and normal stress differences in steady state, are quantitatively reproduced in the whole range of volume fraction. Furthermore, the model is validated against particle pressure measurements that were not used for parameter identification. Even if the proposed constitutive equation for the Cauchy stress tensor is more difficult to interpret than in the minimal model, this study opens way for the use of conformation tensor rheological models in applications where the effect of the second normal stress difference is prominent, like elongational flows or migration phenomenon.

1. Introduction

Concentrated suspensions of non-colloidal particles present two main non-Newtonian rheological trends, namely existence of finite *normal stress differences* and of *transient effects* (e.g., Guazzelli & Pouliquen 2018). (i) Since the early work of Gadala-Maria (1979), *normal stress differences* have been reported and investigated in different flowing geometries (Zarraga *et al.* 2000; Singh & Nott 2003; Couturier *et al.* 2011; Boyer *et al.* 2011; Dbouk *et al.* 2013). These different measurements show that the second normal stress difference N_2 is negative, and that its absolute value grows with volume fraction ϕ. The first normal stress difference N_1 is consistently found to be much smaller, in absolute value, than $|N_2|$. Probably due to these small values, the sign of N_1 remains however debated: For instance, opposite signs were recently measured in the studies of Couturier *et al.* (2011) and Dbouk *et al.* (2013). (ii) Using shear reversal experiments, Gadala-Maria & Acrivos (1980) showed that non-colloidal suspensions develop a *transient behaviour* with *rate-independence*, i.e. no characteristic time. These shear-reversal experiments were

† Email address for correspondence: pierre.saramito@math.cnrs.fr

later revisited by Kolli *et al.* (2002) and Blanc *et al.* (2011). All these authors related the transient effects to the development of microstructure anisotropy under shear flow, and attempted to quantify this anisotropy using the pair distribution function.

Non-Newtonian trends of concentrated suspensions are adequately captured by *particle-based numerical simulations*, which offer additional insights into the physical processes at play. Earliest approaches were based on so-called Stokesian dynamics, in which hydrodynamic interactions are split into far-field and near-field (lubrication) contributions (Brady & Bossis 1985). Numerous studies showed that an essential ingredient to obtain realistic rheological behaviour in these simulations and, in particular, the existence of finite normal-stress differences, is to account for particle contacts through short-range repulsive forces (Nott & Brady 1994; Sierou & Brady 2002). Numerical results also demonstrated frictional interactions should be taken into account to recover correct orders of magnitude for these normal-stress differences, i.e. $|N_1| < |N_2|$ (Sierou & Brady 2002; Mari *et al.* 2014). Similar conclusions concerning the critical role of particle friction were reached by Gallier *et al.* (2014), using a more accurate DNS method to model hydrodynamic interactions. More recently Peters *et al.* (2016) and Chacko *et al.* (2018) were also able to successfully simulate shear-reversal transient effects using DNS and simplified Stokesian dynamics approaches, respectively. These particle-based simulations make it possible to perform numerical experiments and continuously vary physical parameters, thereby providing data that are fully complementary to "real" experiments. However, due to the high demand in computing power, they are still limited to small systems with a relatively low number of particles (a few thousands at most).

Unlike discrete particle-based models, *continuous rheological models* are well suited to simulating large systems. Nevertheless, the elaboration of rheological models able to reproduce both normal-stress differences and transient features has been proved a challenging task (e.g., Denn & Morris 2014). Morris & Boulay (1999) introduced the *suspension balance model*, a continuous model with an explicit expression for the normal stress components (see also Miller & Morris 2006). This model provides relatively accurate predictions for steady state flows, but is unable to account for transient effects.

Transient effects can be described by introducing a *conformation tensor*, denoted $\boldsymbol{b}_e$ in this paper, which represents microstructure anisotropy. Note that conformation tensors are also sometimes referred to as *texture tensors* (see e.g. Lehoucq *et al.* 2015). Hand (1962) formulated general properties for anisotropic fluids, and expressed the Cauchy stress tensor $\boldsymbol{\sigma}$ as a function of both $\boldsymbol{b}_e$ and the strain rate tensor $\dot{\boldsymbol{\gamma}}$. In addition, the conformation tensor $\boldsymbol{b}_e$ needs to obey an evolution equation that ensures rate-independence, i.e. this equation has no characteristic time (e.g., Goddard 1982). Phan-Thien (1995) proposed a differential constitutive equation for the conformation tensor that led, for the first time, to predictions qualitatively in agreement with experimental observations during shear reversal. Goddard (2006) revisited this approach, and proposed a model involving twelve material parameters and two tensors for describing the anisotropy. By a systematic fitting procedure on a limited dataset, he obtained numerical results in quantitative agreement with experiments for transient effects and normal stress differences Stickel *et al.* (2006). proposed a simplified expression for the Cauchy stress tensor, linear versus both the strain rate and the conformation tensors (see also Stickel *et al.* 2007; Yapici *et al.* 2009). While this latter model involves thirteen free parameters, it failed to provide quantitative comparisons with shear reversal experiments: an unexpected sharp spike for both apparent viscosity and normal stress differences was obtained at the time of the reversal. Using a much simpler model involving four

free parameters and a linear evolution evolution for the conformation tensor, Ozenda *et al.* (2018) recently obtained a good quantitative agreement with the shear reversal measurements of Blanc *et al.* (2011) for a wide range of volume fraction ϕ. Furthermore, at the micro-structural scale, the model successfully reproduced both the pair distribution function and the depletion angles measured by Blanc *et al.* (2013). However, this model predicted unphysical normal stress differences.

The objective of this paper is to propose a continuous rheological model that provides quantitative agreement with experiments for both normal stress differences and transient effects, for dilute to highly concentrated suspensions. For that purpose, we revisit and extend the model proposed by Ozenda *et al.* (2018) based on the general expansion of Hand (1962). Section 2 presents the mathematical model. Section 3 is devoted to shear reversal flows. The system of time-dependent equations is expanded for this case, and the stationary solution is explicitly exhibited. The dependence of the material parameters upon volume fraction ϕ is investigated, based on asymptotic analyses in the dilute and highly concentrated limits. In section 4, model predictions are compared with a large number of experimental results regarding both transient effects and steady-state normal stresses. Finally, results are summarised and discussed in section 5.

2. Mathematical model

2.1. *Problem statement*

Following Ozenda *et al.* (2018), let us introduce the *conformation tensor* $\boldsymbol{b}_e = d_0^2\langle \boldsymbol{\ell} \otimes \boldsymbol{\ell}\rangle^{-1}$, where $\boldsymbol{\ell}$ is the branch vector joining the centres of two neighbouring particles and d_0 is the average distance between neighbouring particle centres in an isotropic configuration at rest. In the isotropic configuration at rest, we have $\boldsymbol{b}_e = c_0\boldsymbol{I}$, where $\boldsymbol{I}$ is the identity matrix and c_0 is a dimensionless constant that will be chosen later. For convenience, we introduce the tensor $\boldsymbol{\gamma}_e = \boldsymbol{b}_e - c_0\boldsymbol{I}$, which interprets as the deformation of the micro-structure with respect to rest configuration. As Ozenda *et al.* (2018), we assume a linear evolution for $\boldsymbol{\gamma}_e$:

$$\frac{\mathscr{D}_a\boldsymbol{\gamma}_e}{\mathscr{D}t} + \delta_1|\dot{\boldsymbol{\gamma}}|\boldsymbol{\gamma}_e - \dot{\boldsymbol{\gamma}} = 0 \tag{2.1a}$$

where $\dot{\boldsymbol{\gamma}} = 2D(\boldsymbol{u}) = (\boldsymbol{\nabla u} + \boldsymbol{\nabla u}^T)/2$ is the strain rate tensor, $\boldsymbol{u}$ is the velocity field of the mixture, and δ_1 is a positive dimensionless material parameter. The matrix norm $|\boldsymbol{\xi}|$ is defined by $|\boldsymbol{\xi}|^2 = (\boldsymbol{\xi}{:}\boldsymbol{\xi})/2$ for any matrix $\boldsymbol{\xi}$, with $(\cdot{:}\cdot)$ denoting the double contracted matrix product. We use in (2.1*a*) a general Gordon-Schowalter tensor derivative (Gordon & Schowalter 1972; Saramito 2016):

$$\frac{\mathscr{D}_a\boldsymbol{\gamma}_e}{\mathscr{D}t} = \frac{\partial\boldsymbol{\gamma}_e}{\partial t} + (\boldsymbol{u}.\boldsymbol{\nabla})\boldsymbol{\gamma}_e - W(\boldsymbol{u})\boldsymbol{\gamma}_e + \boldsymbol{\gamma}_e W(\boldsymbol{u}) - a(\dot{\boldsymbol{\gamma}}\boldsymbol{\gamma}_e + \boldsymbol{\gamma}_e\dot{\boldsymbol{\gamma}})$$

where $W(\boldsymbol{u}) = (\boldsymbol{\nabla u} - \boldsymbol{\nabla u}^T)/2$ and $a \in [-1, 1]$ is the parameter of the tensor derivative. Note that Ozenda *et al.* (2018) used an upper-convected derivative, corresponding to $a = 1$. Observe that (2.1*a*) has no characteristic time (Goddard 1982), such that solutions are *rate independent*: In simple shear, changing the amplitude of the strain rate $\dot{\boldsymbol{\gamma}}$ leaves the evolution of $\dot{\boldsymbol{\gamma}}_e$ unchanged when expressed in terms of the dimensionless time $|\dot{\boldsymbol{\gamma}}|t$ (that interprets as a strain).

The Cauchy stress tensor $\boldsymbol{\sigma}$ of the suspension is assumed to express as an analytical function of the two tensorial variables $\dot{\boldsymbol{\gamma}}$ and $\boldsymbol{\gamma}_e$. Following Hand (1962), and through

Cayley-Hamilton theorem, only the zeroth, first and second powers of $\dot{\boldsymbol{\gamma}}$ and $\boldsymbol{\gamma}_e$ can remain in the expression. Furthermore, to preserve the rate-independent property, terms in $\dot{\boldsymbol{\gamma}}^2$ should also be discarded. Here, we consider the following expression for the Cauchy stress tensor:

$$\boldsymbol{\sigma} = -p_b\boldsymbol{I} + \eta\dot{\boldsymbol{\gamma}} + \eta_e\left\{\left(\delta_1|\dot{\boldsymbol{\gamma}}| + \beta_1\frac{\dot{\boldsymbol{\gamma}}:\boldsymbol{\gamma}_e}{2}\right)\boldsymbol{\gamma}_e + \beta_2\left(\frac{\boldsymbol{\gamma}_e^2\dot{\boldsymbol{\gamma}} + \dot{\boldsymbol{\gamma}}\boldsymbol{\gamma}_e^2}{2}\right) + \beta_3|\dot{\boldsymbol{\gamma}}|\boldsymbol{\gamma}_e^2 + \delta_2\left(\frac{\boldsymbol{\gamma}_e\dot{\boldsymbol{\gamma}} + \dot{\boldsymbol{\gamma}}\boldsymbol{\gamma}_e}{2}\right)\right\} \tag{2.1b}$$

where p_b is the pressure of the mixture, η and η_e are characteristic viscosities, and β_1, β_2, β_3 and δ_2 are additional dimensionless material parameters. The terms in factor of δ_1 and δ_2 are linear in $\boldsymbol{\gamma}_e$, while the terms in factor of β_1, β_2 and β_3 are quadratic in $\boldsymbol{\gamma}_e$. Note that when $\beta_2 = \beta_3 = \delta_2 = 0$, the present model coincides with that presented by Ozenda *et al.* (2018).

Constitutive equations (2.1) are coupled with mass and momentum conservations to obtain a closed problem for three unknowns, namely the mixture pressure p_b, the mixture velocity $\boldsymbol{u}$, and the tensor describing the anisotropy of the micro-structure $\boldsymbol{\gamma}_e$:

$$\frac{\mathscr{D}_a\boldsymbol{\gamma}_e}{\mathscr{D}t} + \delta_1|2D(\boldsymbol{u})|\boldsymbol{\gamma}_e - 2D(\boldsymbol{u}) = 0 \tag{2.2a}$$

$$\rho\left(\frac{\partial\boldsymbol{u}}{\partial t} + (\boldsymbol{u}.\boldsymbol{\nabla})\boldsymbol{u}\right) - \mathbf{div}\,\boldsymbol{\sigma} = 0 \tag{2.2b}$$

$$\operatorname{div}\boldsymbol{u} = 0 \tag{2.2c}$$

where the Cauchy stress tensor $\boldsymbol{\sigma}$ is expressed by (2.1*b*). Note that p_b in (2.1*b*) should be regarded as the Lagrange multiplier associated to the incompressibility constraint (2.2*c*). This set of equations is closed by appropriate boundary and initial conditions for $\boldsymbol{u}$ and $\boldsymbol{\gamma}_e$.

As a remark, from (2.2*a*), the conformation tensor $\boldsymbol{b}_e = c_0\boldsymbol{I} + \boldsymbol{\gamma}_e$ satisfies:

$$\frac{\mathscr{D}_a\boldsymbol{b}_e}{\mathscr{D}t} - \frac{\delta_1|2D(\boldsymbol{u})|}{a}\boldsymbol{I} + \delta_1|2D(\boldsymbol{u})|\boldsymbol{b}_e = 2(1-ac_0)D(\boldsymbol{u})$$

By choosing the dimensionless constant as $c_0 = 1/a$, the right-hand-side in the previous relation is zero. In the following, we also assume $a \in]0,1]$. According to Hulsen (1990) and since $\delta_1 > 0$, the conformation tensor $\boldsymbol{b}_e$ is then positive definite at any time, if this property is satisfied at initial time.

3. Simple shear and shear reversal

3.1. *The reduced problem*

Let us consider a simple shear flow: The x axis is in the flow direction and the y axis is in the direction of velocity gradient, such that $\boldsymbol{u}(t,x,y,z) = (u_x(t,y),0,0)$. Let us denote $\dot{\gamma} = \partial_y u_x$ the uniform (scalar) shear rate. Note that $|\dot{\gamma}| = |\dot{\boldsymbol{\gamma}}|$. Evolution equation (2.2*a*)

for $\boldsymbol{\gamma}_e(t)$ reduces to the following system of ordinary differential equations:

$$\partial_t \gamma_{e,xx} - (1+a)\dot{\gamma}\,\gamma_{e,xy} + \delta_1|\dot{\gamma}|\,\gamma_{e,xx} = 0 \tag{3.1a}$$
$$\partial_t \gamma_{e,yy} + (1-a)\dot{\gamma}\,\gamma_{e,xy} + \delta_1|\dot{\gamma}|\,\gamma_{e,yy} = 0 \tag{3.1b}$$
$$\partial_t \gamma_{e,xy} - \frac{1+a}{2}\dot{\gamma}\,\gamma_{e,yy} - \frac{1-a}{2}\dot{\gamma}\,\gamma_{e,xx} + \delta_1|\dot{\gamma}|\,\gamma_{e,xy} = \dot{\gamma} \tag{3.1c}$$
$$\partial_t \gamma_{e,xz} - (1+a)\dot{\gamma}\,\gamma_{e,yz} + \delta_1|\dot{\gamma}|\,\gamma_{e,xz} = 0 \tag{3.1d}$$
$$\partial_t \gamma_{e,yz} + (1-a)\dot{\gamma}\,\gamma_{e,xz} + \delta_1|\dot{\gamma}|\,\gamma_{e,yz} = 0 \tag{3.1e}$$
$$\partial_t \gamma_{e,zz} + \delta_1|\dot{\gamma}|\,\gamma_{e,zz} = 0 \tag{3.1f}$$

We assume here $\gamma_{e,xz} = \gamma_{e,yz} = \gamma_{e,zz} = 0$ at $t = 0$, such that these components remain zero at any time. The constitutive equation (2.1*b*) for $\boldsymbol{\sigma}$ becomes:

$$\begin{aligned}\sigma_{xx} = -p_b + \eta_e \{&(\delta_1|\dot{\gamma}| + \beta_1\dot{\gamma}\gamma_{e,xy})\,\gamma_{e,xx} + \beta_2\dot{\gamma}\,(\gamma_{e,xx} + \gamma_{e,yy})\,\gamma_{e,xy} \\ &+ \beta_3|\dot{\gamma}|\,(\gamma_{e,xx}^2 + \gamma_{e,xy}^2) + \delta_2\dot{\gamma}\gamma_{e,xy}\}\end{aligned} \tag{3.2a}$$
$$\begin{aligned}\sigma_{yy} = -p_b + \eta_e \{&(\delta_1|\dot{\gamma}| + \beta_1\dot{\gamma}\gamma_{e,xy})\,\gamma_{e,yy} + \beta_2\dot{\gamma}\,(\gamma_{e,xx} + \gamma_{e,yy})\,\gamma_{e,xy} \\ &+ \beta_3|\dot{\gamma}|\,(\gamma_{e,xy}^2 + \gamma_{e,yy}^2) + \delta_2\dot{\gamma}\gamma_{e,xy}\}\end{aligned} \tag{3.2b}$$
$$\sigma_{zz} = -p_b \tag{3.2c}$$
$$\begin{aligned}\sigma_{xy} = \eta\dot{\gamma} + \eta_e \Big\{&(\delta_1|\dot{\gamma}| + \beta_1\dot{\gamma}\gamma_{e,xy})\,\gamma_{e,xy} + \frac{\beta_2\dot{\gamma}}{2}\,(\gamma_{e,xx}^2 + \gamma_{e,yy}^2 + 2\gamma_{e,xy}^2) \\ &+ \beta_3|\dot{\gamma}|\,(\gamma_{e,xx} + \gamma_{e,yy})\,\gamma_{e,xy} + \frac{\delta_2\dot{\gamma}}{2}\,(\gamma_{e,xx} + \gamma_{e,yy})\Big\}\end{aligned} \tag{3.2d}$$
$$\sigma_{xz} = \sigma_{yz} = 0 \tag{3.2e}$$

The system (3.1) is linear and admits explicit solutions when the shear rate $\dot{\gamma}$ is given. Explicit expressions of the stress components are then obtained from (3.2). In the following, we will also consider the case of an imposed shear stress σ_{xy}. In this case, numerical solutions of the coupled equations (3.1)-(3.2) are computed using the `lsode` ordinary differential equation solver (Radhakrishnan & Hindmarsh 1993) implemented within the `numpy-scipy` environment (Jones *et al.* 2001–).

3.2. *Explicit solution in steady state*

The steady state solution of (3.1*a*)-(3.1*c*) writes:

$$\gamma_{e,xx} = \frac{1+a}{1-a^2+\delta_1^2} \tag{3.3a}$$
$$\gamma_{e,yy} = \frac{-(1-a)}{1-a^2+\delta_1^2} \tag{3.3b}$$
$$\gamma_{e,xy} = \frac{\delta_1\,\mathrm{sgn}(\dot{\gamma})}{1-a^2+\delta_1^2} \tag{3.3c}$$

The apparent viscosity $\eta_{app} = \sigma_{xy}/\dot{\gamma}$ and the normal stress differences $N_1 = \sigma_{xx} - \sigma_{yy}$ and $N_2 = \sigma_{yy} - \sigma_{zz}$ associated to the steady state solution are then easily deduced from

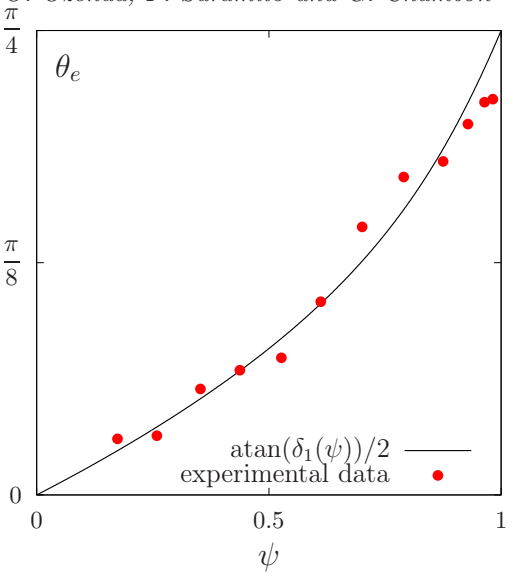

FIGURE 1. Depletion angle θ_e versus reduced volume fraction ψ: comparison between model prediction (3.5a) and experimental measurements of Blanc *et al.* (2013).

(3.2a)-(3.2d):

$$\eta_{app} = \eta + \frac{\eta_e}{1-a^2+\delta_1^2}\left(\delta_1^2 + a\delta_2 + \frac{\delta_1^2\beta_1 + \left(1+a^2+\delta_1^2\right)\beta_2 + 2a\delta_1\beta_3}{1-a^2+\delta_1^2}\right) \tag{3.4a}$$

$$N_1 = \frac{2\eta_e|\dot\gamma|}{1-a^2+\delta_1^2}\left(\delta_1 + \frac{\delta_1\beta_1 + 2a\beta_3}{1-a^2+\delta_1^2}\right) \tag{3.4b}$$

$$N_2 = \frac{\eta_e|\dot\gamma|}{1-a^2+\delta_1^2}\left(\delta_1(-1+a+\delta_2) + \frac{-(1-a)\delta_1\beta_1 + 2a\delta_1\beta_2 + \left((1-a)^2+\delta_1^2\right)\beta_3}{1-a^2+\delta_1^2}\right) \tag{3.4c}$$

We also define the particle pressure $p_p = p - p_b$, where $p = -\mathrm{tr}(\boldsymbol{\sigma})/3$ is the total pressure of the suspension. In steady state:

$$p_p = -\frac{2\eta_e|\dot\gamma|}{3(1-a^2+\delta_1^2)}\left(\delta_1(a+\delta_2) + \frac{a\delta_1\left(\beta_1+2\beta_2\right) + \left(1+a^2+\delta_1^2\right)\beta_3}{1-a^2+\delta_1^2}\right) \tag{3.4d}$$

3.3. *Dependence of material parameters upon volume fraction*

The model presented in section 2 involves eight material parameters: two viscosities η and η_e, and six dimensionless parameters a, δ_1, δ_2, β_1, β_2 and β_3. Preliminary tests to fit experimental data for different volume fractions ϕ (see § 4), showed that all these parameters except a appear to vary with ϕ. Following these preliminary investigations, we assumed a to be independent of ϕ, and the seven remaining parameters to depend only upon the reduced volume fraction $\psi = \phi/\phi_m$, where ϕ_m denotes the maximal volume fraction of the suspension. This latter assumption was required to apply the model to different experimental datasets. In practice, ϕ_m can vary between 0.53 and 0.64, typically, depending on particle shape, roughness, etc (Guazzelli & Pouliquen 2018).

As shown in appendix A, the parameter δ_1 is related to the *depletion angle* θ_e, i.e. the

angle between the x axis and the direction of the eigenvector associated to the largest eigenvalue of $\boldsymbol{\gamma}_e$, as follows: $\delta_1 = \tan(2\theta_e)$. Based on the experimental measurements of θ_e provided by Blanc *et al.* (2013), the following dependence law is proposed for δ_1 (figure 1):

$$\delta_1(\psi) = \bar{\delta}_1 \left((1-\psi)^{-1} - (1-b\psi) \right) \tag{3.5a}$$

where $\bar{\delta}_1$ and b are positive constants independent of ψ. Identification from experimental data leads to $\bar{\delta}_1 \approx 0.27$ and $b \approx 2$. Observe that $\delta_1(0) = 0$ and $\delta_1(1) = \infty$, such that the model predicts $\theta_e(0) = 0$ and $\theta_e(1) = \pi/4$.

To be consistent with numerous existing results (Maron & Pierce 1956; Morris & Boulay 1999; Guazzelli & Pouliquen 2018), the apparent viscosity η_{app} and the second normal stress difference N_2 should behave as $(1-\psi)^{-2}$ in the $\psi \to 1$ limit. In addition, we expect $\eta_e = 0$ in the Newtonian limit $\psi = 0$. Accordingly, the following dependence laws are considered for the viscosities η and η_e:

$$\eta(\psi) = \eta_0 \left(1 - \omega + \psi \left(\frac{5}{2}\phi_m - 2\omega \right) + \omega(1-\psi)^{-2} \right) \tag{3.5b}$$

$$\eta_e(\psi) = \eta_0 \bar{\eta}_e \psi (1-\psi)^{-2} \tag{3.5c}$$

where η_0 is the viscosity of the suspending fluid, and $\bar{\eta}_e > 0$ is a constant independent of ψ. The constant $\omega \in]0,1[$ is introduced in (3.5*b*) in order to recover Einstein (1906)'s relation when $\psi \to 0$ (see §3.4).

Like η_e, the parameters δ_2, β_1, β_2 and β_3 should all vanish when $\psi = 0$, i.e. the mixture reduces to a Newtonian fluid. For simplicity, we consider that δ_2 is proportional to δ_1. We also assume that parameters β_i behave as $(1-\psi)^{-2}$ when $\psi \to 1$. Finally, the following dependence laws are postulated:

$$\delta_2(\psi) = \bar{\delta}_2 \left((1-\psi)^{-1} - (1-b\psi) \right) \tag{3.5d}$$

$$\beta_i(\psi) = \bar{\beta}_i \left((1-\psi)^{-1} - 1 \right)^2, \quad i = 1,2,3 \tag{3.5e}$$

where $\bar{\delta}_2$ and $\bar{\beta}_1$, $\bar{\beta}_2$, $\bar{\beta}_3$ are constants independent of ψ.

At this stage, the suspension model involves nine constants independent of ψ, namely $\bar{\delta}_1$, b, a, ω, $\bar{\eta}_e$, $\bar{\delta}_2$, $\bar{\beta}_1$, $\bar{\beta}_2$, and $\bar{\beta}_3$. While δ_1 and b have already been identified, the seven other constants remain to be determined from experimental data. Note that with the dependence laws (3.5*b*)-(3.5*c*) for η and η_e, we obtain from (3.4) that the normal stress ratios

$$\alpha_1 = \frac{N_1}{\eta_{app}\,|\dot{\gamma}|} \quad \text{and} \quad \alpha_2 = \frac{N_2}{\eta_{app}\,|\dot{\gamma}|}$$

are independent of the viscosity of the suspending fluid η_0, in agreement with experiments (Dbouk *et al.* 2013; Guazzelli & Pouliquen 2018).

3.4. *Dilute and concentrated limits*

For the dilute limit $\psi \to 0$, a second-order Taylor expansion of (3.4*a*) leads to the following expression for apparent viscosity η_{app}:

$$\eta_{app} = \eta_0 \left(1 + \frac{5}{2}\phi_m \psi + \left(\frac{3\omega}{2} + \frac{a(1+b)\bar{\delta}_2 \bar{\eta}_e}{(1-a^2)} \right) \psi^2 \right) + O\left(\psi^3\right) \tag{3.6a}$$

At first order in ψ, the model agrees with Einstein (1906)'s relation $\eta_{app} \approx \eta_0(1 + 5\phi/2)$. The different constants associated to micro-structure evolution, a, b, $\bar{\eta}_e$ and $\bar{\delta}_2$, appear

only at second order,consistently with the asymptotic development of Batchelor & Green (1972).

In the concentrated limit $\psi \to 1$, the expansion of η_{app} writes:

$$\eta_{app} = \eta_0 \bar{\eta}_1 (1-\psi)^{-2} + O\left((1-\psi)^{-1}\right) \tag{3.6b}$$
$$\text{with } \bar{\eta}_1 = \left(\omega + \left(1 + \frac{\bar{\beta}_1 + \bar{\beta}_2}{\bar{\delta}_1^2}\right)\bar{\eta}_e\right)$$

Hence, η_{app} grows as $(1-\psi)^{-2}$, as expected (Maron & Pierce 1956).

Let us now turn to the asymptotic behaviour of normal stress ratios α_1 and α_2 and of particle pressure p_p. In the dilute limit $\psi \to 0$, from (3.4), we obtain:

$$\alpha_1 = = \frac{2\bar{\eta}_e \bar{\delta}_1 (1+b)}{1-a^2}\psi^2 + O\left(\psi^3\right)$$
$$\alpha_2 = = -\frac{(1-a)\bar{\eta}_e \bar{\delta}_1 (1+b)}{1-a^2}\psi^2 + O\left(\psi^3\right)$$
$$\frac{p_p}{\eta_{app}\,|\dot{\gamma}|} = -\frac{2a\bar{\eta}_e \bar{\delta}_1 (1+b)}{3(1-a^2)}\psi^2 + O\left(\psi^3\right)$$

Observe that α_1, α_2 and p_p all vanish when $\psi = 0$, as expected. Moreover, we obtain $\alpha_1 \geqslant 0$ and $\alpha_2 \leqslant 0$ when $\psi \to 0$. This sign for α_2 is consistent with experimental observations (Couturier *et al.* 2011; Dbouk *et al.* 2013).

In the concentrated limit $\psi \to 1$, the expansions of normal stress ratios and particle pressure write:

$$\alpha_1 = \frac{2\bar{\eta}_e}{\bar{\eta}_1 \bar{\delta}_1}\left(1 + \frac{\bar{\beta}_1}{\bar{\delta}_1^2}\right)(1-\psi) + O\left((1-\psi)^2\right)$$
$$\alpha_2 = -\frac{\bar{\eta}_e}{\bar{\eta}_1}\left(\frac{-\bar{\delta}_1\bar{\delta}_2 - \bar{\beta}_3}{\bar{\delta}_1^2}\right) + O\left(1-\psi\right)$$
$$\frac{p_p}{\eta_{app}\,|\dot{\gamma}|} = \frac{2\bar{\eta}_e}{3\bar{\eta}_1}\left(\frac{-\bar{\delta}_1\bar{\delta}_2 - \bar{\beta}_3}{\bar{\delta}_1^2}\right) + O\left(1-\psi\right)$$

Note that α_1 vanishes when $\psi \to 1$. On the contrary, α_2 tends to a constant for $\psi \to 1$, in agreement with experiments (Leighton & Acrivos 1987; Guazzelli & Pouliquen 2018). Furthermore, it is sufficient to assume $\bar{\delta}_2 < 0$ and $\bar{\beta}_3 \leqslant 0$ to obtain $\alpha_2 \leqslant 0$.

4. Quantitative comparisons with experiments

As explained above, the present model is in qualitative agreement with experimental observations in both the dilute and concentrated limits. More quantitatively, we now identify the different model constants using two experimental datasets characterised by varying volume fractions ϕ in the range $[0.2, 0.5]$ and different experimental protocols:

- Blanc *et al.* (2011) performed measurements of transient apparent viscosity during shear reversal for five different values of volume fraction ϕ. These authors used a suspending fluid of viscosity $\eta_0 = 1.02$ Pa.s, PMMA spheres of radius $r_p = 16$ μm, and reported a relatively low maximum volume fraction $\phi_m = 0.535$ presumably due to the presence of a residual cellulosic surfactant.

a	b	ω	$\bar{\eta}_e$	$\bar{\delta}_1$	$\bar{\delta}_2$	$\bar{\beta}_1$	$\bar{\beta}_2$	$\bar{\beta}_3$
0.60	2.0	0.28	0.21	0.27	−0.80	0.050	0.45	−0.19

TABLE 1. Set of nine dimensionless model constants identified from experimental data.

• Dbouk *et al.* (2013) presented measurements of normal stress differences in steady state, using different suspending fluids with viscosity $0.05 \leqslant \eta_0 \leqslant 0.5$ Pa.s, polystyrene spheres of radius $r_p = 70$ μm, and reported a maximal volume fraction $\phi_m = 0.58$.

For these two datasets, values of ϕ were rescaled in terms of reduced volume fractions $\psi = \phi/\phi_m$ using the provided values of ϕ_m.

As described in appendix B, the set of seven model constants $\{a,\ \omega,\ \bar{\eta}_e, \bar{\delta}_2,\ \bar{\beta}_1,\ \bar{\beta}_2\ \ \bar{\beta}_3\}$ was *globally* identified from these two experimental datasets. The obtained values are grouped in table 1. Note that a first attempt at a direct global identification of the constants failed. Accordingly, we had to allow for slight discrepancies between the values of material parameters associated to steady state and to transient experiments, respectively, and to introduce a corresponding penalisation term in the fitting cost function. Details of the minimisation procedure are explained appendix B.

Figure 2 presents direct comparisons with the experimental data of Blanc *et al.* (2011), namely evolution of transient apparent viscosity $\eta_{app}(t)$ versus strain $\gamma(t) = \int_0^t |\dot{\gamma}(s)|\mathrm{d}s$, for different volume fractions ϕ. Let us recall that the experiments were performed at imposed shear stress, while $\dot{\gamma}(t)$ varies. Observe the good agreement between model predictions and experimental measurements for all values of ϕ. The different successive phases present in the measurements, namely the initial brutal drop in apparent viscosity, the smooth evolution to a minimum, and the relaxation to steady state, are all quantitatively reproduced. For $\phi = 0.30$, the model predicts a slight overshoot in apparent viscosity, which is not visible in the data. As shown in figure 3, the steady-state apparent viscosity predicted by (3.4*a*) is also in excellent agreement with experimental data .

Figure 4 presents the evolution of steady-state normal stress ratios as a function of reduced volume fraction ψ. In addition to the data of Dbouk *et al.* (2013) used for identification, model predictions are also compared against the data of Couturier *et al.* (2011). These latter authors used a suspending fluid of viscosity $\eta_0 = 2.15$ Pa.s, polystyrene spheres of radius $r_p = 35$ μm, and reported a maximal volume fraction $\phi_m = 0.62$. The model successfully captures the main features of the normal stress measurements obtained in the two studies, namely $N_2 < 0$ and $|N_1| < |N_2|$. In addition, predictions for the second normal stress ratio α_2 are in quantitative agreement with both experimental datasets (figure 4-right). Regarding the first normal stress difference, measurements show contradictory signs and trends with ψ (figure 4-left). The present model predicts positive values for N_1, in agreement with Dbouk *et al.* (2013), and non-monotonic variations of the ratio α_1 with ψ, consistently with the dilute and concentrated limits $\alpha_1(0) = \alpha(1) = 0$ (see § 3.4).

Finally, the model was also assessed against particle pressure measurements obtained by Deboeuf *et al.* (2009). These authors used a suspending fluid of viscosity $\eta_0 = 3$ Pa.s and

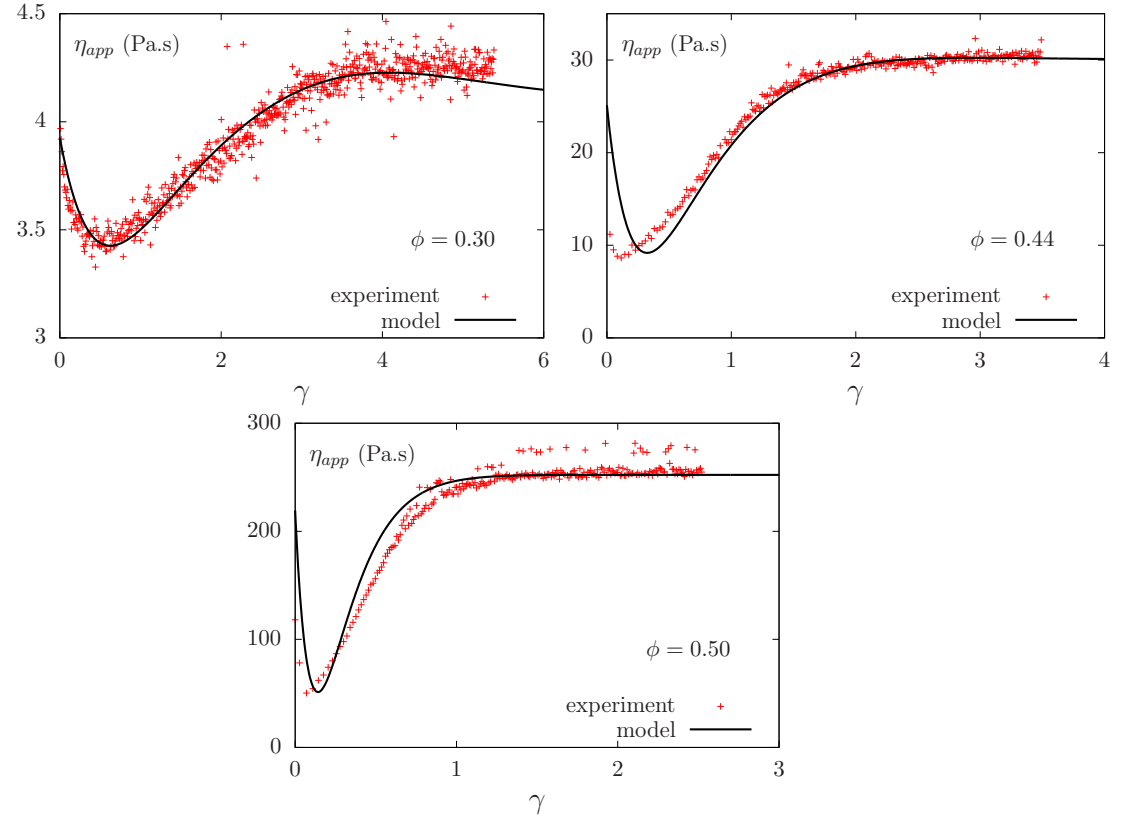

FIGURE 2. Apparent viscosity η_{app} versus strain γ during shear reversal: comparison between model prediction and experimental measurements of Blanc *et al.* (2011) for various volume fractions ϕ.

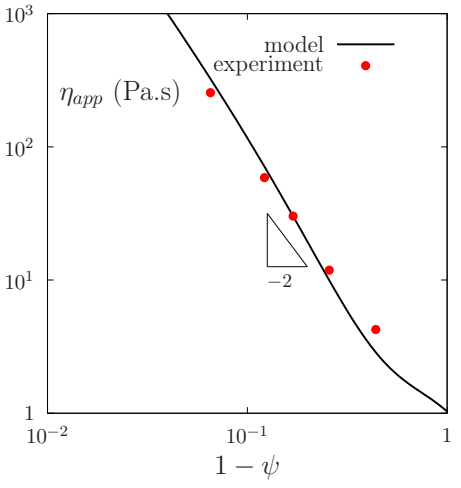

FIGURE 3. Steady-state apparent viscosity η_{app} versus reduced volume fraction ψ: comparison between model predictions and experimental measurements of Blanc *et al.* (2011).

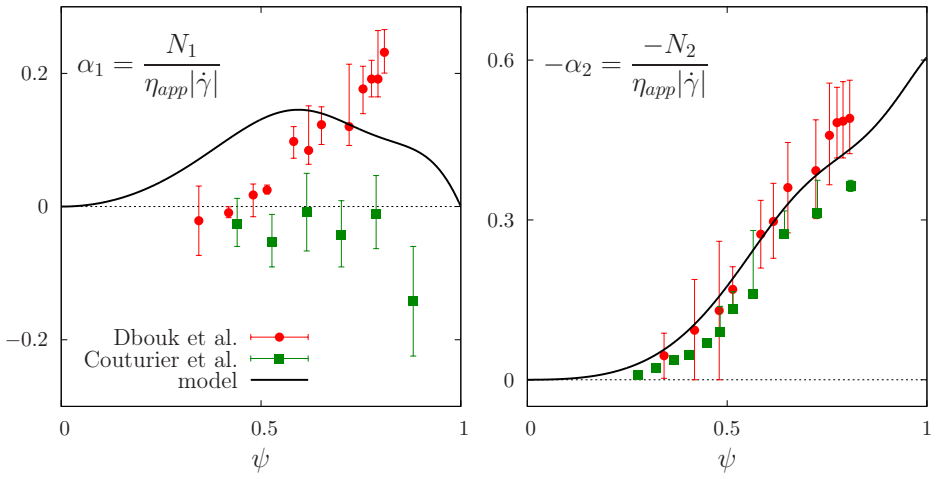

FIGURE 4. Steady-state normal stress ratios α_1 and α_2 versus reduced volume fraction ψ: comparison between model predictions and experimental measurements of Dbouk *et al.* (2013) and Couturier *et al.* (2011).

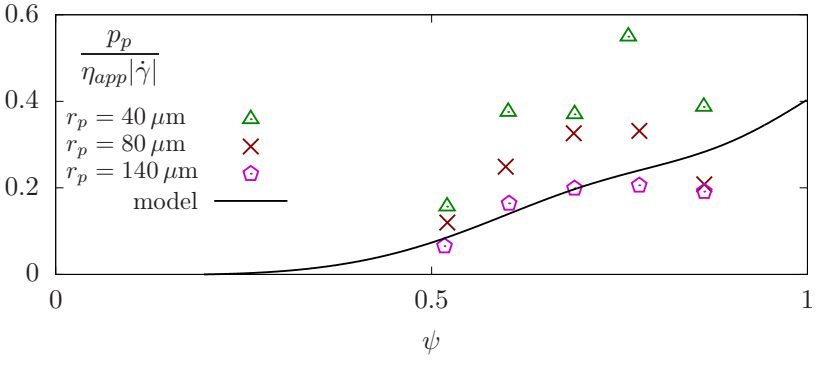

FIGURE 5. Steady-state particle pressure p_p versus reduced volume fraction ψ: comparison between model predictions and experimental measurements of Deboeuf *et al.* (2009) for three different particle radii r_p.

differents sets of particles with radii ranging between 40 and 140 μm. As they did not provide the value of maximum volume fraction ϕ_m, we used $\phi_m = 0.58$ to rescale their data. As shown in figure 5, model predictions are here also in good agreement with the experimental measurements. Note that the values of model constants are unchanged with respect to those used for the previous comparisons, even though this latter dataset was not used for identification. This remarkable result validates the introduction of reduced volume fraction $\psi = \phi/\phi_m$ in the dependence laws for the material parameters in §3.3. The model constants involved in these dependence laws (see table 1) can be regarded, at least to a first approximation, as independent of the experimental conditions. The influence of experimental conditions is then only encoded in the value of maximum volume fraction ϕ_m.

5. Discussion and conclusions

An improved rheological model for non-colloidal suspensions of hard spheres, involving the evolution of a conformation tensor, was presented. The model extends that of Ozenda *et al.* (2018) in several respects: While the structure of the linear evolution equation (2.1*a*) for the conformation tensor is unchanged, a more general Gordon-Schowalter tensor derivative is used, with a material parameter $a \in]0, 1[$. In addition, the expression of the Cauchy stress tensor (2.1*b*) is complemented by three new non-linear terms. These changes are necessary to accurately predict both the transient evolution of apparent viscosity during shear reversal, and the values of second normal stress difference N_2 in steady state. Moreover, the present model also predicts $|N_1| < |N_2|$, in agreement with observations, and was shown to quantitatively reproduce particle pressure measurements.

The model was compared to four experimental datasets involving different suspending fluids and particle sizes. To that aim, the material parameters were all expressed in terms of reduced volume fraction $\psi = \phi/\phi_m$, where the maximum volume fraction ϕ_m varies among the experiments. The good agreement observed with the different datasets suggests that the rheological model, together with the constants given in table 1, can be applied to large range of non-colloidal suspensions. Appendix C presents a systematic sensitivity study with respect to these different model constants. It appears that all the additional terms in the Cauchy stress equation have a significant influence on model predictions, i.e. none of them can be omitted without significantly degrading the match with observations. We also note the existence of non-trivial couplings between the different terms, which explain the difficulties encountered for model identification (see appendix B). A more detailed investigation of alternative optimisation solutions, with the aim of proposing a more physical interpretation of the different terms and a more systematic identification procedure, shall be tackled in future work.

The ability of the presented model to predict accurate normal stresses opens way to continuous computations of elongational or more complex flows of suspensions. The model could also be coupled to an evolution law for the volume fraction in order to address migration phenomena (Miller & Morris 2006). As a preamble to such computations on complex configurations, a more in-depth analysis of the mathematical and thermodynamical properties of the model needs however to be undertaken.

REFERENCES

Batchelor, G. K. & Green, J. T. 1972 The determination of the bulk stress in a suspension of spherical particles to order c^2. *J. Fluid Mech.* **56** (03), 401–427.

Blanc, F., Lemaire, E., Meunier, A. & Peters, F. 2013 Microstructure in sheared non-brownian concentrated suspensions. *J. Rheol.* **57** (1), 273–292.

Blanc, F., Peters, F. & Lemaire, E. 2011 Local transient rheological behavior of concentrated suspensions. *J. Rheol.* **55** (4), 835–854.

Boyer, F., Pouliquen, O. & Guazzelli, E 2011 Dense suspensions in rotating-rod flows: normal stresses and particle migration. *Journal of Fluid Mechanics* **686**, 5–25.

Brady, John F & Bossis, Georges 1985 The rheology of concentrated suspensions of spheres in simple shear flow by numerical simulation. *J. Fluid Mech.* **155**, 105–129.

Chacko, Rahul N, Mari, Romain, Fielding, Suzanne M & Cates, Michael E 2018 Shear reversal in dense suspensions: the challenge to fabric evolution models from simulation data. *J. Fluid Mech.* **847**, 700–734.

Couturier, E., Boyer, F., Pouliquen, O. & Guazzelli, E 2011 Suspensions in a tilted trough: second normal stress difference. *J. Fluid Mech.* **686**, 26–39.

Dbouk, T., Lobry, L. & Lemaire, E. 2013 Normal stresses in concentrated non-brownian suspensions. *J. Fluid Mech.* **715**, 239–272.

Deboeuf, A., Gauthier, G., Martin, J., Yurkovetsky, Y. & Morris, J. F. 2009 Particle pressure in a sheared suspension: a bridge from osmosis to granular dilatancy. *Phys. Rev. Let.* **102** (10), 108301.

Denn, M. M. & Morris, J. F. 2014 Rheology of non-brownian suspensions. *Annual review of chemical and biomolecular engineering* **5**, 203–228.

Einstein, A. 1906 Eine neue bestimmung der moleküldimensionen. *Ann. Phys. ser. 4* **19**, 289–306.

Gadala-Maria, F 1979 The rheology of concentrated suspensions. PhD thesis, Stanford University.

Gadala-Maria, F. & Acrivos, A. 1980 Shear-induced structure in a concentrated suspension of solid spheres. *J. Rheol.* **24** (6), 799–814.

Gallier, S., Lemaire, E., Peters, F. & Lobry, L. 2014 Rheology of sheared suspensions of rough frictional particles. *J. of Fluid Mech.* **757**, 514–549.

Goddard, J. D. 1982 Memory materials without characteristic time and their relation to the rheology of certain particle suspensions. *Adv. Coll. Interf. Sci.* **17** (1), 241–262.

Goddard, J. D. 2006 A dissipative anisotropic fluid model for non-colloidal particle dispersions. *J. Fluid Mech.* **568**, 1–17.

Gordon, R. J. & Schowalter, W. R. 1972 Anisotropic fluid theory: a different approach to the dumbbell theory of dilute polymer solutions. *J. Rheol.* **16**, 79–97.

Guazzelli, E. & Pouliquen, O. 2018 Rheology of dense granular suspensions. *J. Fluid Mech.* **852**, P1.

Hand, G. L. 1962 A theory of anisotropic fluids. *J. Fluid Mech.* **13** (1), 33–46.

Hulsen, M. A. 1990 A sufficient condition for a positive definite configuration tensor in differential models. *J. Non-Newt. Flui Mech.* **38** (1), 93–100.

Jones, E., Oliphant, T., Peterson, P. & others 2001– SciPy: Open source scientific tools for Python. [Online; accessed ¡today¿].

Kolli, V. G., Pollauf, E. J. & Gadala-Maria, F. 2002 Transient normal stress response in a concentrated suspension of spherical particles. *J. Rheol* **46** (1), 321–334.

Lehoucq, R., Weiss, J., Dubrulle, B., Amon, A., le Bouil, A., Crassous, J., Amitrano, D. & Graner, F. 2015 Analysis of image vs. position, scale and direction reveals pattern texture anisotropy. *Frontiers in Physics* **2**, 84.

Leighton, D. & Acrivos, A. 1987 The shear-induced migration of particles in concentrated suspensions. *J. Fluid Mech.* **181**, 415–439.

Mari, R., Seto, R., Morris, J. F. & Denn, M. M. 2014 Shear thickening, frictionless and frictional rheologies in non-brownian suspensions. *J. Rheol.* **58** (6), 1693–1724.

Maron, S. H. & Pierce, P. E. 1956 Application of Ree-Eyring generalized flow theory to suspensions of spherical particles. *J. Colloid Sci.* **11** (1), 80–95.

Miller, Ryan M & Morris, Jeffrey F 2006 Normal stress-driven migration and axial development in pressure-driven flow of concentrated suspensions. *J. Non-Newt. Fluid Mech.* **135** (2-3), 149–165.

More, J. J., Garbow, B. S. & Hillstrom, K. E. 1980 User guide for minpack-1.[in fortran]. *Tech. Rep.*.

Morris, J. F. & Boulay, F. 1999 Curvilinear flows of noncolloidal suspensions: The role of normal stresses. *J. Rheol.* **43** (5), 1213–1237.

Newville, Matthew, Stensitzki, Till, Allen, Daniel B, Rawlik, Michal, Ingargiola, Antonino & Nelson, Andrew 2016 Lmfit: non-linear least-square minimization and curve-fitting for python. *Astro. Source Code Lib.* .

Nott, P. R. & Brady, J. F. 1994 Pressure-driven flow of suspensions: simulation and theory. *J. Fluid Mech.* **275**, 157–199.

Ozenda, O., Saramito, P. & Chambon, G. 2018 A new rate-independent tensorial model for suspensions of noncolloidal rigid particles in newtonian fluids. *J. Rheol.* **62** (4), 889–903.

Peters, F., Ghigliotti, G., Gallier, S., Blanc, F., Lemaire, E. & Lobry, L. 2016 Rheology of non-brownian suspensions of rough frictional particles under shear reversal: A numerical study. *J. Rheol.* **60** (4), 715–732.

Phan-Thien, N. 1995 Constitutive equation for concentrated suspensions in Newtonian liquids. *J. Rheol.* **39** (4), 679–695.

Radhakrishnan, K. & Hindmarsh, A. C. 1993 Description and use of lsode, the livermore solver for ordinary differential equations .

Saramito, P. 2016 *Complex fluids: modelling and algorithms*. Springer.

Sierou, A. & Brady, J. F. 2002 Rheology and microstructure in concentrated noncolloidal suspensions. *J. Rheol.* **46**, 1031–1056.

Singh, A. & Nott, P. R. 2003 Experimental measurements of the normal stresses in sheared stokesian suspensions. *J. Fluid Mech.* **490**, 293–320.

Stickel, J. J., Phillips, R. J. & Powell, R. L. 2006 A constitutive model for microstructure and total stress in particulate suspensions. *J. Rheol.* **50** (4), 379–413.

Stickel, J. J., Phillips, R. J. & Powell, R. L. 2007 Application of a constitutive model for particulate suspensions: Time-dependent viscometric flows. *J. Rheol.* **51** (6), 1271–1302.

Yapici, K., Powell, R. L. & Phillips, R. J. 2009 Particle migration and suspension structure in steady and oscillatory plane Poiseuille flow. *Phys. Fluids* **21** (5), 053302.

Zarraga, I. E., Hill, D. A. & Leighton Jr, D. T. 2000 The characterization of the total stress of concentrated suspensions of noncolloidal spheres in newtonian fluids. *J. Rheol.* **44** (2), 185–220.

Appendix A. Eigen directions of $\boldsymbol{\gamma}_e$

We prove here that, in stationary simple shear flow, the depletion angle, i.e. the angle between the x axis and the direction of the eigenvector associated to the largest eigenvalue of $\boldsymbol{\gamma}_e$, expresses as:

$$\delta_1 = \tan(2\theta_e) \tag{A 1}$$

From (3.3*a*)-(3.3*c*), eigenvalues of $\boldsymbol{\gamma}_e$, denoted as $\lambda_{min} \leqslant \lambda_{max}$, are both non-zero and write:

$$\lambda_{min} = \frac{\delta_1^{-1}}{1+\delta_1^{-2}(1-a^2)}\left(a\delta_1^{-1} - \left(\delta_1^{-2}+1\right)^{1/2}\right)$$
$$\lambda_{max} = \frac{\delta_1^{-1}}{1+\delta_1^{-2}(1-a^2)}\left(a\delta_1^{-1} + \left(\delta_1^{-2}+1\right)^{1/2}\right)$$

The corresponding eigenvectors are:

$$\boldsymbol{v}_{min} = \begin{bmatrix} \delta_1^{-1} - \left(\delta_1^{-2}+1\right)^{1/2} \\ 1 \end{bmatrix} \qquad \boldsymbol{v}_{max} = \begin{bmatrix} 1 \\ \left(\delta_1^{-2}+1\right)^{1/2} - \delta_1^{-1} \end{bmatrix}$$

Accordingly, we obtain:

$$\theta_e = \operatorname{atan}\left(\left(\delta_1^{-2}+1\right)^{1/2} - \delta_1^{-1}\right) = \frac{\operatorname{atan}(\delta_1)}{2}$$

which is equivalent to (A 1). Observe that $\forall\ \delta_1 > 0,\ \theta_e \in]0, \pi/4[$.

Remark that, while the eigenvalues of $\boldsymbol{\gamma}_e$ depend on the parameter a of the tensor derivative, the eigenvectors are independent thereof. Hence, all the relations between microstructure orientation and model parameters derived in Ozenda *et al.* (2018), notably (A 1), remain unchanged in the present model.

Appendix B. Identification of model constants

The rheological model involves seven constants to be identified: a, ω, $\bar{\eta}_e$, $\bar{\beta}_1$, $\bar{\beta}_2$, $\bar{\beta}_3$, $\bar{\delta}_2$. Let us define the following cost function:

$$J_0 = \frac{w_{s,0}}{\psi_5 - \psi_1} \int_{\psi_1}^{\psi_5} |\eta_{app}(\psi) - \eta_{app}^{obs}(\psi)| \, \mathrm{d}\psi + \sum_{i=1}^{2} \frac{w_{s,i}}{\psi_m} \int_0^{\psi_m} |\alpha_i(\psi) - \alpha_i^{obs}(\psi)| \, \mathrm{d}\psi$$
$$+ \sum_{k=1}^{5} \frac{w_{t,k}}{\gamma_k} \int_0^{\gamma_k} |\eta_{app}(\psi_k, \gamma) - \eta_{app,k}^{obs}(\gamma)| \, \mathrm{d}\gamma$$

The function $\eta_{app}^{obs}(\psi)$ is a piecewise-constant interpolation of steady-state values of apparent viscosity measured by Blanc *et al.* (2011) for $\psi \in [\psi_1, \psi_5]$, with $\psi_1 = 0.56$ and $\psi_5 = 0.93$ the range of reduced volume fraction explored in the experiments (see table 2). The functions $\alpha_1^{obs}(\psi)$ and $\alpha_2^{obs}(\psi)$ are piecewise-constant interpolations of steady-state values of normal stress ratios measured by Dbouk *et al.* (2013) for $\psi \in [0, \psi_m]$, with $\psi_m = 0.81$ the maximal reduced volume fraction reached in the experiments. The functions $\eta_{app,k}^{obs}(\gamma)$, $k = 1 \dots 5$, represent the transient evolutions of apparent viscosity during the five shear reversal experiments of Blanc *et al.* (2011) characterised by reduced volume fractions ψ_k (see table 2). Here, γ_k, $k = 1 \dots 5$, represent the maximal strain reached in each experiment. Lastly, the function $\eta_{app}(\psi, \gamma)$ is associated to the transient solution of the model, while the functions $\eta_{app}(\psi)$, $\alpha_1(\psi)$, and $\alpha_2(\psi)$ are associated to the steady-state solution. The factors $w_{s,i}$ and $w_{t,k}$ are relative weights associated to the cost function J_0.

First attempts at identifying model constants by direct minimisation of J_0 turned out unsuccessful. We thus had to relax the assumption of identical material parameters in the transient and steady-state regimes. Let us introduce the relaxed material parameters $\beta_{1,k}^{rlx}$, $\beta_{2,k}^{rlx}$, $\beta_{3,k}^{rlx}$, $\delta_{2,k}^{rlx}$, $\eta_{e,k}^{rlx}$, η_k^{rlx}, for the five transient experiments $k = 1 \dots 5$. Accordingly, a supplementary term is added to the previous cost function:

$$J = J_0 + \frac{1}{\psi_5 - \psi_1} \int_{\psi_1}^{\psi_5} \big\{ w_{\beta_1} |\beta_1(\psi) - \beta_1^{rlx}(\psi)| + w_{\beta_2} |\beta_2(\psi) - \beta_2^{rlx}(\psi)|$$
$$+ w_{\beta_3} |\beta_3(\psi) - \beta_3^{rlx}(\psi)| + w_{\delta_2} |\delta_2(\psi) - \delta_2^{rlx}(\psi)|$$
$$+ w_{\eta_e} |\eta_e(\psi) - \eta_e^{rlx}(\psi)| + w_\eta |\eta(\psi) - \eta^{rlx}(\psi)| \big\} \, \mathrm{d}\psi \qquad \text{(B 1)}$$

The functions $\beta_1^{rlx}(\psi)$, $\beta_2^{rlx}(\psi)$, $\beta_3^{rlx}(\psi)$, $\delta_2^{rlx}(\psi)$, $\eta_e^{rlx}(\psi)$, and $\eta^{rlx}(\psi)$ are piecewise-constant interpolations of the corresponding relaxed material parameters for $\psi \in [\psi_1, \psi_5]$. Conversely, the functions $\beta_1(\psi)$, $\beta_2(\psi)$, $\beta_3(\psi)$, $\delta_2(\psi)$, $\eta(\psi)$, $\eta_e(\psi)$ are given by the dependence laws (3.5), which involve the constants $\bar{\beta}_1$, $\bar{\beta}_2$, $\bar{\beta}_3$, $\bar{\delta}_2$, ω and $\bar{\eta}_e$. Lastly, w_{β_1}, w_{β_2}, w_{β_3} , w_{δ_2}, w_{η_e}, w_{eta} are additional weight factors. Note also that, in J_0, the function $\eta_{app}(\psi_k, \gamma)$ is now computed with the relaxed material parameters.

The cost function J is minimised on the argument set containing model constants and relaxed material parameters. In total, the global identification of the model thus involves a set of 37 arguments. Numerical minimisation was performed with a Levenberg-Marquardt method (More *et al.* 1980), using the optimisation library `lmfit` (Newville *et al.* 2016). Convergence was difficult to achieve due to the existence of several local minima. In practice we start by fixing all the weights in J_0 to 1, and all the weights associated to

Exp (n^0)	ψ_k	$\delta_{1,k}^{rlx}$	η_k^{rlx} (Pa.s)	$\eta_{e,k}^{rlx}$ (Pa.s)	$\beta_{1,k}^{rlx}$	$\beta_{2,k}^{rlx}$	$\beta_{3,k}^{rlx}$	$\delta_{2,k}^{rlx}$
1	0.56	0.65	3.6	0.53	0.093	1.3	−0.32	−2.0
2	0.74	1.2	6.8	2.5	0.37	3.9	−1.1	−4.0
3	0.82	1.7	10	5.7	0.94	11	−2.4	−5.3
4	0.88	2.4	15	9.7	2.7	24	−5.5	−6.3
5	0.93	4.3	56	37	10	90	−42	−12

TABLE 2. Relaxed material parameters for the five transient experiments.

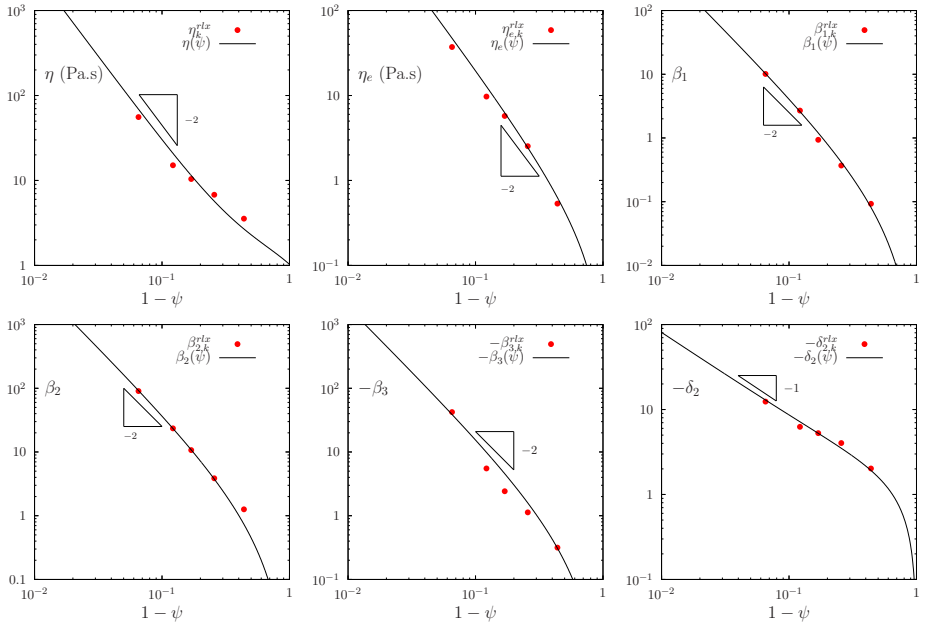

FIGURE 6. Relaxed material parameters compared with the dependence laws (3.5), as a function of reduced volume fraction ψ.

relaxation to 10^{-3}. The obtained solution is then iteratively enhanced by progressively increasing the relaxation weights.

Identified model constants are indicated in table 1, while relaxed material parameters for the five transient experiments are given in table 2. Figure 6 shows a comparison between these relaxed material parameters and the values obtained from dependence laws (3.5) involving the model constants. Note the good overall agreement, showing that relaxation has only a small influence on the final result.

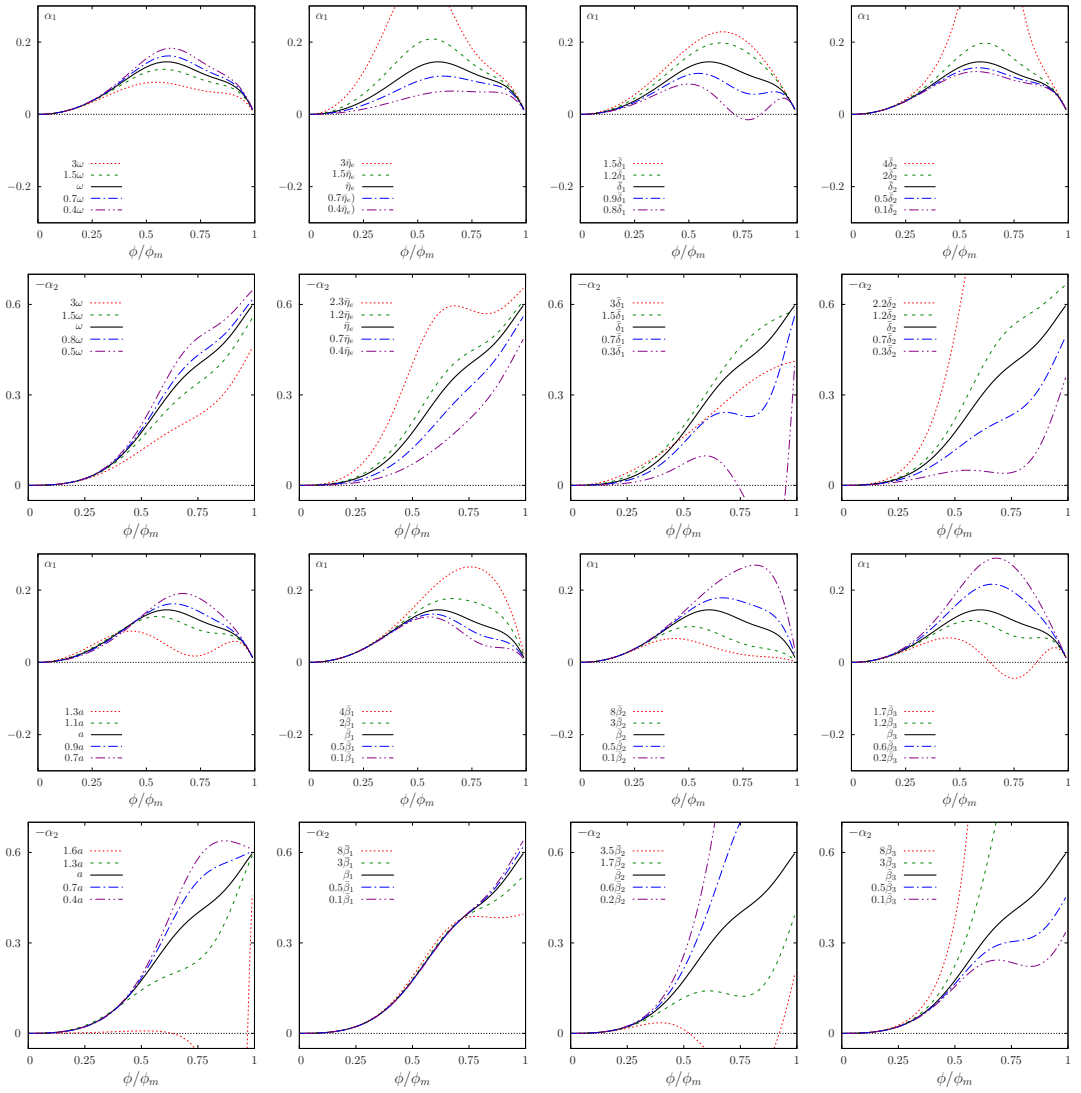

FIGURE 7. Sensitivity of normal stress ratios α_1 and α_2 with respect to model constants. Each of the constants was varied around the reference values indicated in table 1.

Appendix C. Sensitivity study

Figure 7 shows the sensitivity of steady-state normal stress ratios α_1 and α_2 with respect to the eight model constants a, ω, $\bar{\eta}_e$, $\bar{\beta}_1$, $\bar{\beta}_2$, $\bar{\beta}_3$, $\bar{\delta}_1$, $\bar{\delta}_2$. Similarly, figure 8 presents a sensitivity study for the transient apparent viscosity during shear reversal.

Overall, the ratios α_1 and α_2 are only weakly sensitive to the constants ω and $\bar{\beta}_1$ (figure 7). Conversely, variations of the other constants can lead to significant qualitative changes, such as non-monotonous variations of α_2 with ψ. Note also that an unphysical prediction $|\alpha_1| \geqslant |\alpha_2|$ is obtained when values of $\bar{\delta}_2$ or $\bar{\beta}_3$ are close to zero, or when $a \approx 1$. Similarly an unphysical change of sign of α_2 is observed when a or $\bar{\delta}_1$ are large, or when $\bar{\beta}_2$ is close to zero. These results show that the introduction of the four new constants a, $\bar{\delta}_2$, $\bar{\beta}_2$ and

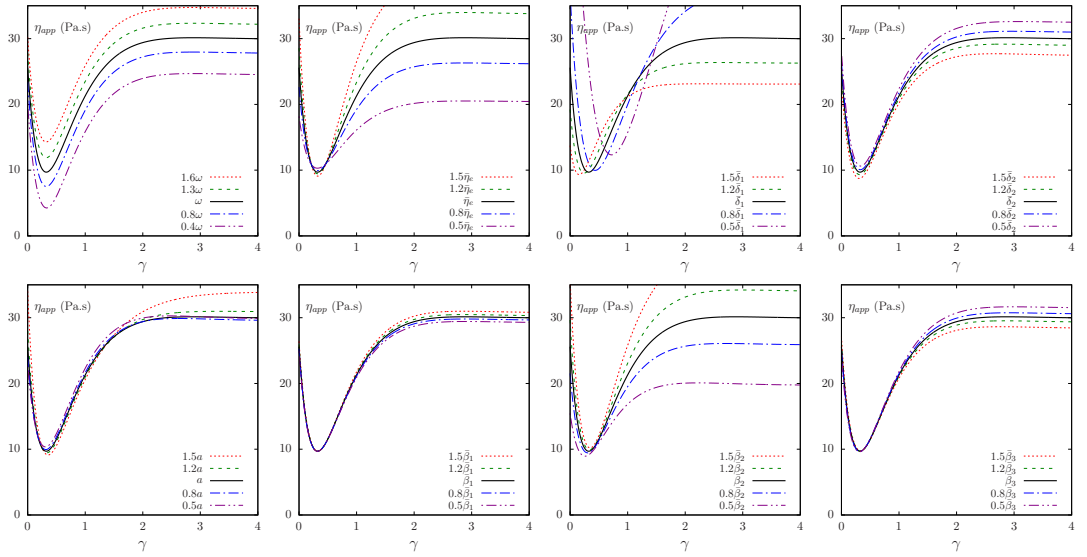

FIGURE 8. Sensitivity of transient apparent viscosity η_{app} with respect to model constants. Each of the constants was varied around the reference values indicated in table 1.

$\bar{\beta}_3$, compared to the model proposed by Ozenda *et al.* (2018), is effectively necessary to obtain correct normal stress predictions.

Figure 8 shows a weak sensitivity of the transient apparent viscosity with respect to model constants a, $\bar{\beta}_1$, $\bar{\beta}_3$ and $\bar{\delta}_2$. Conversely, as already observed by Ozenda *et al.* (2018), the constant ω has a direct influence on the value of the apparent viscosity minimum, while $\bar{\delta}_1$ affects the minimum position. Lastly, $\bar{\eta}_e$, $\bar{\delta}_1$and $\bar{\beta}_2$ affect the steady-state regime.